



Contents lists available at ScienceDirect

Journal of Alloys and Compounds

journal homepage: www.elsevier.com/locate/jalcom

Quasielastic neutron scattering study of tetrahydroborate anion dynamical perturbations in sodium borohydride due to partial halide anion substitution

Nina Verdal ^{a,b}, Terrence J. Udovic ^{a,*}, John J. Rush ^{a,b}, Alexander V. Skripov ^c

^a NIST Center for Neutron Research, National Institute of Standards and Technology, Gaithersburg, MD 20899-6102, USA

^b Department of Materials Science and Engineering, University of Maryland, College Park, MD 20742-2115, USA

^c Institute of Metal Physics, Ural Branch of the Russian Academy of Sciences, Ekaterinburg 620990, Russia

ARTICLE INFO

Article history:

Available online xxx

Keywords:

Complex hydrides
Quasielastic neutron scattering
Reorientational dynamics
Sodium borohydride
Sodium chloride
Sodium iodide

ABSTRACT

Equimolar $\text{NaBH}_4\text{-NaX}$ ($\text{X} = \text{Cl}$ and I) solid solutions were synthesized to study, via quasielastic neutron scattering, the effect of partial halide anion substitution on the reorientational dynamics of tetrahydroborate (BH_4^-) anions in NaBH_4 . The BH_4^- reorientational mobility increased in the order of $\text{NaBH}_4\text{-NaCl}$, NaBH_4 , and $\text{NaBH}_4\text{-NaI}$, which corresponded with expanding face-centered-cubic lattices accommodating the respective increasing sizes of the Cl^- , BH_4^- , and I^- anions. The BH_4^- anions in $\text{NaBH}_4\text{-NaCl}$ were found (at least above 400 K) to undergo ‘cubic’ tumbling motions with the four H atoms per anion visiting all eight corners of a cube, similar to what was previously observed for NaBH_4 . In contrast, the BH_4^- anions in $\text{NaBH}_4\text{-NaI}$ were found to undergo something more akin to ‘tetrahedral’ tumbling motions, where the H atoms visit all four corners of a tetrahedron. Despite a noticeable softening of the BH_4^- torsional energies with increasing lattice constant amongst NaBH_4 and the two solid solutions, all three compounds exhibited similar activation energies for reorientation of about $11\text{--}12\text{ kJ mol}^{-1}$.

© 2014 Published by Elsevier B.V.

1. Introduction

Compounds containing tetrahydroborate (BH_4^-) anions are potentially important materials for a variety of applications such as solid-state hydrogen storage [1] and fast-ion conduction [2]. Aside from their ionic character, such compounds often possess interesting molecular dynamics due to the propensity of the BH_4^- anions to undergo relatively facile reorientational motions, with jump frequencies that vary widely depending on their crystal environment and that can easily surpass 10^{12} s^{-1} at technologically relevant temperatures [3–5]. Often, their dynamical properties can be sensitive indicators of departures from bulk thermodynamic properties. For example, LiBH_4 nanoconfined in a controlled-pore carbon framework was observed to exhibit two fractions of dynamically different BH_4^- anions, one highly mobile fraction associated with LiBH_4 near the pore interface and another slower, more bulk-like fraction in the interior of the pore [5,6]. In general, the ability to observe and differentiate such dynamical information can lead to an increased understanding of thermodynamic and kinetic phenomena of complex systems on a more fundamental molecular level.

In the present paper, we investigate by quasielastic neutron scattering (QENS) the perturbation to BH_4^- reorientational dynamics in the light-alkali-metal borohydride NaBH_4 modified by partial halide (Cl^- and I^-) anion substitution. Analogous studies on hexagonal LiBH_4 diluted with LiI have suggested similar reorientational mechanisms for both neat and partially iodide-substituted LiBH_4 , (i.e., rapid diffusive-like reorientational jumps of three H atoms around the local BH_4^- trigonal axis concomitant with slower jump exchanges of these H atoms with the fourth axial H atom) but with increased BH_4^- anion reorientational mobility for the latter iodide-substituted compounds [7,8].

NaBH_4 is known to undergo an order–disorder transition near 190 K [9]. Below this temperature, the compound exhibits a tetragonal lattice with orientationally ordered BH_4^- anions. Above this temperature, it transforms to a face-centered-cubic (fcc) structure with orientationally disordered BH_4^- anions [10,11]. Each anion possesses two equally probable orientations superimposed to form a cube of eight H atoms, each with 50% occupancy, with a B atom at the center. Partial substitution of the BH_4^- anions with either Cl^- or I^- anions leads to a disordered fcc solid solution phase [12–14] (see Fig. 1). At these high halide concentrations and in the absence of an ordered sublattice of BH_4^- and halide anions, it is reasonable to assume that the disordered solid-solution phase will already be

* Corresponding author.

comprised of both significant substitutional and orientational disorder at the lowest temperatures, precluding any possible further entropically driven order–disorder transition such as occurs for pure NaBH_4 at higher temperatures. The respective room-temperature cubic NaCl , NaBH_4 , and NaI lattice constants of 5.642 Å [12], 6.157 Å [14], and 6.469 Å [14] reflect the VI-coordinate Shannon crystal radius of the Na^+ cation (1.16 Å) and the relative increase in the Shannon crystal radii of the anions from Cl^- (1.67 Å) to BH_4^- (1.92 Å) to I^- (2.06 Å) [15,16]. Hence, partial Cl^- and I^- substitution leads solid-solution compounds with respectively smaller and larger lattice constants than for NaBH_4 , which may impact BH_4^- reorientational mechanism and mobility.

2. Materials and methods

All sample manipulations were performed inside a He-filled glovebox. Equimolar $\text{Na}^{11}\text{BH}_4\text{-NaX}$ ($\text{X} = \text{Cl}$ and I) solid solutions were synthesized by ball-milling 1:1 mixtures of $\text{Na}^{11}\text{BH}_4$ (Katchem [17]) and NaX (NaCl and NaI , both $\geq 99.5\%$, Aldrich) under a He atmosphere using a Fritsch Pulverisette no. 7 ball mill. ^{11}B -enriched NaBH_4 was used to avoid the large neutron absorption cross section of ^{10}B present in natural boron. (N.B., we have dropped the isotope designation throughout the rest of this paper for simplicity.) Eight 10 mm diameter stainless steel balls were used in a 12 ml stainless steel jar with a sample-to-ball mass ratio of either 1:30 ($\text{NaBH}_4\text{-NaI}$) or 1:20 ($\text{NaBH}_4\text{-NaCl}$). For $\text{NaBH}_4\text{-NaI}$, the 4 h total processing time was comprised of a repetitive two-step sequence: i.e., 2 min with the mill on (200 Hz) followed by 2 min with the mill off. For $\text{NaBH}_4\text{-NaCl}$, the 24 h total processing time consisted of cycles of 5 min milling with 2 min rest. After milling, the samples were annealed for 4 d at 533 K in an inert He gas environment. The homogeneities of the resulting solid solutions were confirmed by X-ray powder diffraction (XRD) using a Rigaku Ultima III X-ray diffractometer with a $\text{Cu K}\alpha$ source. For neutron scattering measurements, all samples were loaded into annular-shaped Al foil packets (yielding close to 10% scatterers) and further sealed inside cylindrical Al cells. During measurements, temperatures were regulated with a He closed-cycle refrigerator.

All neutron scattering measurements were performed at the NIST Center for Neutron Research. Neutron elastic scattering fixed-window scans (FWSs) (and QENS spectra for $\text{NaBH}_4\text{-NaI}$) were collected on the High-Flux Backscattering Spectrometer (HFBS) [18], which operates at an incident neutron wavelength of 6.27 Å and an instrumental resolution of about 0.8 μeV full width at half maximum (FWHM). Each displayed FWS was formed by summing over all detectors for a total momentum transfer (Q) range of $0.2 \text{ Å}^{-1} < Q < 1.75 \text{ Å}^{-1}$. QENS spectra were also collected on the Disk-Chopper Time-of-Flight Spectrometer (DCS) [19] using

incident neutron wavelengths of 6 Å, yielding an instrumental resolution of 30 μeV FWHM and a maximum Q value of 1.97 Å^{-1} ; 4.1 Å, yielding an instrumental resolution of 80 μeV FWHM and a maximum Q value of 2.88 Å^{-1} ; and 2.75 Å, yielding an instrumental resolution of 275 μeV FWHM and a maximum Q value of 4.29 Å^{-1} . Neutron vibrational spectra were obtained on the Filter-Analyzer Neutron Spectrometer (FANS) [20] using both the pyrolytic graphite PG(002) and $\text{Cu}(220)$ monochromators to cover the neutron energy transfer ranges of 10–32 meV and 32–180 meV, respectively. Horizontal collimations of 20° of arc were used before and after the monochromator. Instrumental resolutions varied from around 1.2 meV FWHM below 32 meV to about 3% of the energy transfer above 32 meV. The neutron scattering data were reduced and analyzed using the DAVE [21] software package. The unit cell schematic was created with the VESTA software package [22]. All error bars in the figures denote $\pm 1 \sigma$.

3. Quasielastic neutron scattering methodology

In a QENS experiment, monoenergetic neutrons are impinged onto a sample and the energies and intensities of the resulting scattered neutrons near zero energy transfer are measured as a function of Q . Ideally, the elastically scattered neutrons would yield a delta function at zero energy transfer, but in reality, this function is convoluted with the instrumental resolution function and is more Gaussian-like. Since the incoherent neutron scattering cross section for hydrogen is much higher than other elements, scattering due to H atoms will dominate the observed incoherent scattering intensity (between the Bragg peaks). For the compounds under consideration, we only have to consider the scattering from the H atoms associated with the BH_4^- anions. At low temperatures, the BH_4^- anions are relatively immobile with respect to the instrumental resolution, and the incoherent scattering from the H atoms yields only an elastic peak. As the temperature is increased, the reorientational jump rates of the BH_4^- anions increase to the point that the neutron is able to ‘sense’ these motions and a portion of the elastic peak begins to broaden into one or more Lorentzian components (quasielastic scattering), the number and fraction depending on the reorientational mechanism. As the temperature increases further, the quasielastic scattering becomes ever broader and eventually collapses into the baseline, leaving only the elastic component observable.

One useful QENS measurement on a backscattering spectrometer such as HFBS is a fixed window scan (FWS), where we record the scattering intensity at zero energy transfer as a function of temperature. FWSs are useful, in general, for establishing the relative mobilities of hydrogenous species in different solid-state materials [23]. At the lower temperatures, if the reorientational jump rates of the BH_4^- anions are less than about 10^8 s^{-1} , no quasielastic broadening is observable, all of the scattering is elastic, and the FWS intensity will be relatively high. In this temperature region, there is only a gradual drop due to the effect of the Debye–Waller factor. As the temperature is raised further, the jump frequencies eventually become greater than 10^8 s^{-1} , some of the elastic peak intensity becomes quasielastic (i.e., broadened) and the resulting FWS intensity will begin to decrease significantly until the quasielastic component disappears into the baseline (at jump rates $> 10^{10} \text{ s}^{-1}$). At this point, only the elastic component remains, and the reduced FWS intensity again continues its gradual drop with further increases in temperature.

In addition to what we learn from FWS measurements, we can potentially determine the BH_4^- reorientational mechanism by analyzing, in detail, the Q dependence of the QENS spectra. Typically, we calculate the elastic incoherent structure factor (EISF) as a function of Q . The EISF is defined as the ratio of purely elastic scattering intensity to the total scattering intensity (i.e., elastic + quasielastic scattering intensity). The EISF functional behavior with Q is sensitive to the reorientational mechanism. By plotting EISF vs. Q and comparing to different reorientational model functions, we can often draw reasonable conclusions concerning the predominant reorientational mechanism.

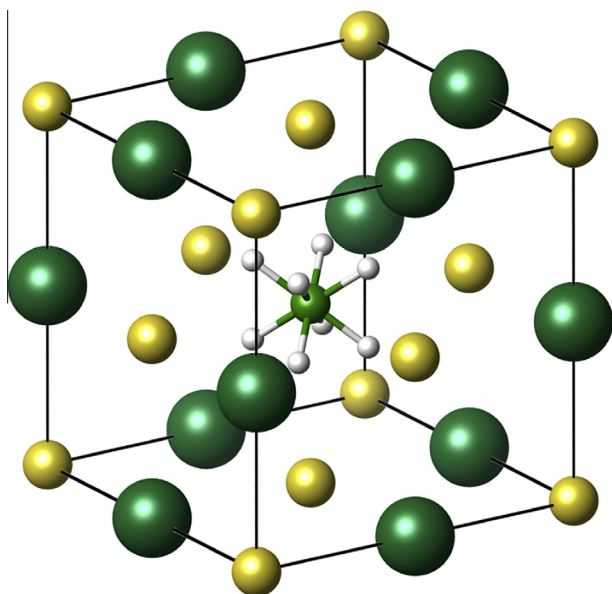


Fig. 1. Schematic of the BH_4^- anion centered within the disordered fcc lattice of $\text{NaBH}_4\text{-NaX}$ ($\text{X} = \text{Cl}$, BH_4 , or I). Na, X, B, and H are denoted by gold, large green, small green, and white spheres, respectively. It is assumed that all BH_4^- anions possess diffraction-average orientational disorder between two positions as observed for NaBH_4 above 190 K, resulting in 50% H atom occupation of the eight cube corners. (For interpretation of the references to color in this figure legend, the reader is referred to the web version of this article.)

Finally, as the quasielastic linewidth is a measure of the jump rate, by plotting the linewidth vs. inverse temperature in an Arrhenius fashion, we can obtain the activation energy for reorientation E_a from the slope of $-E_a/k$, where k is Boltzmann's constant.

4. Results and discussion

Fig. 2 displays a comparison of the FWSs for $\text{NaBH}_4\text{-NaCl}$ and $\text{NaBH}_4\text{-NaI}$. Since pure NaBH_4 is in its ordered tetragonal structure below 190 K, it is only meaningful to compare the FWS of the two isotopic, disordered cubic mixed compounds below this temperature. For the best comparison, the scans were rescaled and shifted appropriately to line up the intensities for the two compounds at both the lowest and highest temperatures in order to correct for differences in sample size and any intensity variations due to possible differences in reorientational mechanisms. It is seen that, as the anion size increases, the reorientational jump rate increases at a given temperature (thus lowering the elastic scattering intensity), and the temperature corresponding to the onset of rapid reorientations decreases. Hence, there is a likely trend in relative BH_4^- mobilities with lattice constant. In particular, between the two mixed compounds, BH_4^- is relatively less mobile in $\text{NaBH}_4\text{-NaCl}$ where the lattice is relatively smaller. This makes sense sterically, since a larger lattice translates to a larger interstitial volume and less constrictive nearest-neighbor interactions, on average, for the rotating BH_4^- anions. This is consistent with what is observed for hexagonal LiBH_4 with or without partial I^- anion substitution [8,24,25]. This trend with lattice size also agrees with the relative BH_4^- mobilities observed for the series of alkali-metal borohydrides [23]. It should be noted that no FWS discontinuity due to an order–disorder phase transition, as seen for NaBH_4 at 190 K [23], is evident for the two solid-solution compounds.

Fig. 3 compares the EISFs determined from DCS data measured out to Q values of 4.29 \AA^{-1} for $\text{NaBH}_4\text{-NaCl}$ and $\text{NaBH}_4\text{-NaI}$ at several higher temperatures corresponding to similar quasielastic linewidths (i.e., reorientational jump frequencies on the order of 10^{12} s^{-1}), with model curves corresponding to various reorientational mechanisms. Here we consider only physically reasonable models for the particular BH_4^- site geometry, namely, (i) twofold and threefold reorientational jumps around a single symmetry axis, (ii) reorientational jumps amongst the four corners of a

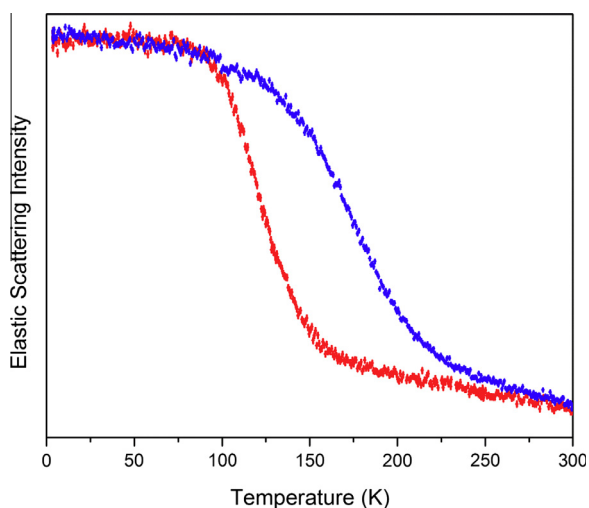


Fig. 2. A comparison of neutron elastic scattering fixed-window scans for $\text{NaBH}_4\text{-NaCl}$ (blue) and $\text{NaBH}_4\text{-NaI}$ (red), summed over all detectors ($0.2 \text{ \AA}^{-1} < Q < 1.75 \text{ \AA}^{-1}$) and both offset and scaled appropriately to align all data at both low and high temperatures. (For interpretation of the references to color in this figure legend, the reader is referred to the web version of this article.)

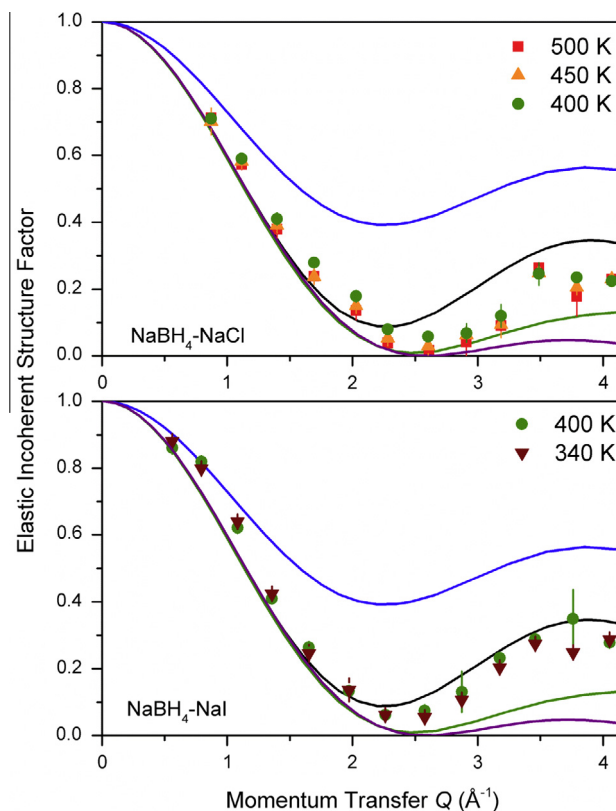


Fig. 3. EISF vs. Q data for $\text{NaBH}_4\text{-NaCl}$ and $\text{NaBH}_4\text{-NaI}$ at several temperatures in comparison with various curves associated with different jump reorientation models (in descending order): twofold and/or threefold uniaxial jumps (blue), tetrahedral tumbling (black), cubic tumbling (green), and isotropic rotational diffusion (purple). (For interpretation of the references to color in this figure legend, the reader is referred to the web version of this article.)

tetrahedron (tetrahedral tumbling); (iii) reorientational jumps amongst the eight corners of a cube (cubic tumbling); and (iv) isotropic rotational diffusion. The functional forms for these reorientational models are described in the Appendix A. For $\text{NaBH}_4\text{-NaCl}$, the data suggest that the BH_4^- anions are undergoing a reorientational mechanism approaching cubic tumbling. This is consistent with what has been previously observed for BH_4^- reorientations in disordered NaBH_4 [26,27], where diffraction indeed indicates a cubic arrangement of H atom positions around each B atom.

Interestingly, the situation for $\text{NaBH}_4\text{-NaI}$ is somewhat different. The EISF data for this compound suggest that the BH_4^- anions are undergoing predominantly tetrahedral tumbling, although the downward trend of the datapoints also suggests that the anions are starting to experience some cubic tumbling on the resolution time-scale of the instrument. This is not inconsistent with the notion of a diffraction-average cubic H atom arrangement around each B atom. Diffraction only gives a composite snapshot of the BH_4^- anion orientations averaged over all unit cells and provides no information concerning the dynamical evolution of individual BH_4^- anions. QENS fills in this gap. For $\text{NaBH}_4\text{-NaCl}$ and NaBH_4 , QENS tells us that the H atoms from individual BH_4^- anions tend to tumble, for the most part, amongst the eight corners of a cube, at least on the DCS timescale. In contrast, for $\text{NaBH}_4\text{-NaI}$, H atoms from individual BH_4^- anions seem to more often favor a particular crystallographic orientation within the lattice, jumping amongst tetrahedral corners a number of times before changing their preferred orientation to the other disordered crystallographic orientation, after which they commence a new series of tetrahedral tumbling motions. Together these two crystallographic

orientations yield a diffraction-average cube of H atoms. Yet, on the DCS timescale, these orientations are ‘dynamically’ separate since the instrument cannot detect the much slower jumps between the two configurations.

We again note that the predominant mechanisms for these two solid-solution compounds are compared at similar jump frequencies but at only one overlapping temperature of 400 K. It would be interesting to extend these EISF measurements for both compounds down to lower temperatures at lower jump frequencies to more thoroughly document the temperature-dependent progression, if any, of the respective reorientational mechanisms. Since we have only made high- Q measurements at these higher temperatures to date, further measurements are needed. Indeed, the mechanistic differences between the two halide-substituted compounds are intriguing and worthy of future investigation.

Fig. 4 illustrates the Arrhenius plots of linewidth vs. inverse temperature for all three compounds (in the same disordered cubic

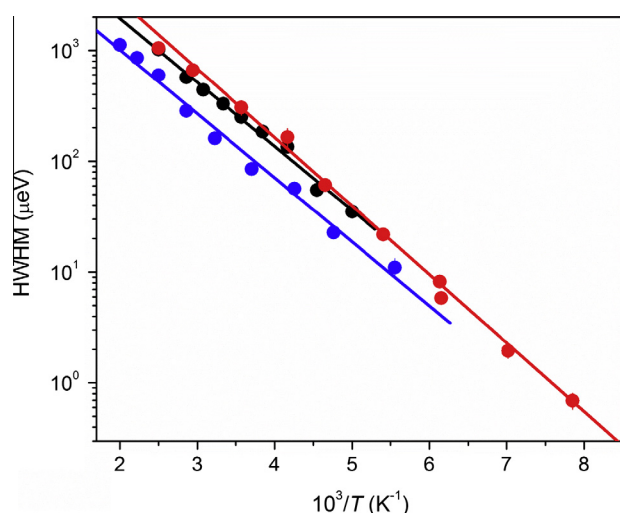


Fig. 4. Arrhenius plots of quasielastic linewidth (HWHM) vs. T^{-1} for $\text{NaBH}_4\text{-NaCl}$ (blue) and $\text{NaBH}_4\text{-NaI}$ (red) in comparison with that observed previously for NaBH_4 (black, from [27]) in its disorder cubic phase. The three lowest-temperature points for $\text{NaBH}_4\text{-NaI}$ were measured on HFBS. Activation energies for reorientation are extracted from the slopes. (For interpretation of the references to color in this figure legend, the reader is referred to the web version of this article.)

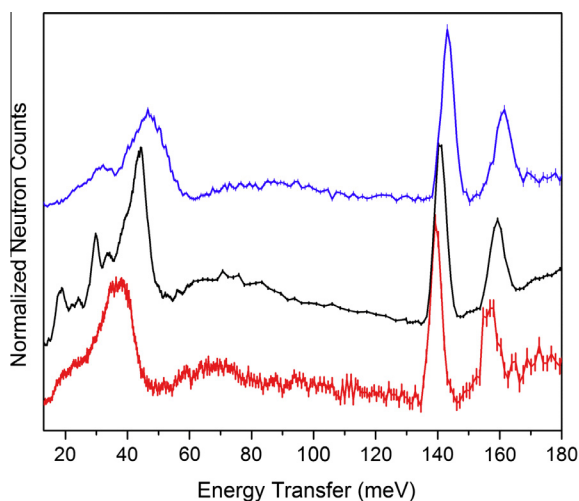


Fig. 5. A comparison of neutron vibrational spectra at 4 K for $\text{NaBH}_4\text{-NaCl}$ (blue), NaBH_4 (black, data above 32 meV from [27]), and $\text{NaBH}_4\text{-NaI}$ (red). (For interpretation of the references to color in this figure legend, the reader is referred to the web version of this article.)

structure) from the QENS data. The relative vertical line shifts reflect the relative mobilities of the compounds as inferred by the FWSs in Fig. 2. There is roughly a factor of two difference in reorientational rates between $\text{NaBH}_4\text{-NaCl}$ and $\text{NaBH}_4\text{-NaI}$, with intermediate rates observed for NaBH_4 . It is interesting that the activation energy for reorientation E_a is found to be very similar for each compound: $11.1(4) \text{ kJ mol}^{-1}$ [$114(4) \text{ meV}$], $11.9(5) \text{ kJ mol}^{-1}$ [$123(5) \text{ meV}$], and $11.7(3) \text{ kJ mol}^{-1}$ [$121(3) \text{ meV}$] for $\text{NaBH}_4\text{-NaCl}$, NaBH_4 [27], and $\text{NaBH}_4\text{-NaI}$, respectively. This seems somewhat surprising since one might reasonably expect a larger, less constrictive BH_4^- anion interstitial site to have a lower barrier to reorientation. Indeed, the neutron vibrational spectra of the three compounds in Fig. 5, although measured at 4 K where there is more of a propensity for orientational ordering and zero reorientational mobility on a neutron timescale, nonetheless indicate some softening of the BH_4^- torsional bands between 30 meV and 60 meV and of the BH_4^- bending modes between 130 meV and 170 meV, as expected for increasing lattice size going from $\text{NaBH}_4\text{-NaCl}$ to NaBH_4 to $\text{NaBH}_4\text{-NaI}$. Apparently, differences in the curvature near the bottom of the H potential well, which lead to minor variations in the phonon energies, may not be predictive of differences in the curvature higher up the potential well or in the ultimate barrier height. First-principles calculations are needed to investigate this phenomenon in more detail.

It should be noted that, because these solid-solution compounds are disordered, they will possess a distribution of BH_4^- environments, each with its own potential energy landscape. Therefore, there is most likely a distribution of phonon energies, jump rates, and activation energy barriers to consider, and the present results represent average values of these parameters. Indeed, there is evidence in Fig. 5 of broadened BH_4^- torsional energy bands for $\text{NaBH}_4\text{-NaCl}$ and $\text{NaBH}_4\text{-NaI}$ compared to that of NaBH_4 due to the inherent lattice disorder of these solid-solution compounds. Thus one should be somewhat cautious of overinterpreting the QENS-derived activation energies, since it assumes that the QENS spectra capture the entire distribution of quasielastic scattering linewidths at each temperature with a single ‘distribution-averaged’ Lorentzian that reflects the average reorientational mobility. This may not be entirely accurate. Even with the expected distribution of anion site environments in these compounds, it is still noteworthy that we are able to perform a reasonable mechanistic analysis of the reorientational dynamics using the average jump rates derived from QENS measurements.

5. Conclusions

We have shown by QENS measurements that BH_4^- reorientational mobility in the high-temperature disordered phase of NaBH_4 was perturbed by partial substitution of the BH_4^- anion with either smaller Cl^- or larger I^- anions. The increase in BH_4^- anion mobility correlated with an increase in the fcc lattice constant (i.e., an increase in the available BH_4^- site volume) due to the corresponding average sizes of the anions. Some differences in BH_4^- reorientational mechanisms were observed for $\text{NaBH}_4\text{-NaCl}$ and $\text{NaBH}_4\text{-NaI}$ in the mobility region of $10^{12} \text{ jumps s}^{-1}$, the former displaying more cubic tumbling behavior, similar to that of NaBH_4 , and the latter more tetrahedral tumbling behavior. $\text{NaBH}_4\text{-NaCl}$, NaBH_4 , and $\text{NaBH}_4\text{-NaI}$ all displayed similar QENS-derived activation energies for reorientation ($11\text{--}12 \text{ kJ mol}^{-1}$). Spectral smearing of the BH_4^- torsional vibrational bands for the mixed compounds compared to that for NaBH_4 corroborated the substitutionally disordered nature of the mixed compounds. The results of additional high- Q measurements at lower temperatures and mobilities for the mixed compounds, as well as a comparison of all QENS results with those from complementary NMR measurements are forthcoming.

Acknowledgements

This work was partially supported by the DOE EERE under Grant No. DE-EE0002978, the Russian Foundation for Basic Research under Grant No. 12-03-00078, the U.S. Civilian Research & Development Foundation (CRDF Global) under Award No. RUP1-7076-EK-12, and the National Science Foundation under Cooperative Agreement No. OISE-9531011. This work utilized facilities supported in part by the National Science Foundation under Agreement DMR-0944772.

Appendix A

The following equations describe the Q -dependence of the EISF for different BH_4^- reorientation mechanisms considered in the text, assuming a perfect BH_4^- tetrahedron with a B–H bond distance $d_{\text{B-H}} = 1.22 \text{ \AA}$ and an H–H bond distance $d_{\text{H-H}} = 1.99 \text{ \AA}$ [27] ($N.B.$, $d_{\text{H-H}} = (8/3)^{1/2} d_{\text{B-H}}$), and where $j_0(x) = \sin(x)/x$.

For twofold or threefold reorientational jumps around a single respective C_2 or C_3 anion symmetry axis [28]:

$$\text{EISF} = \frac{1}{2} [1 + j_0(Qd_{\text{H-H}})]. \quad (1)$$

For reorientational jumps amongst the four corners of a tetrahedron (tetrahedral tumbling) [29]:

$$\text{EISF} = \frac{1}{4} [1 + 3j_0(Qd_{\text{H-H}})]. \quad (2)$$

For reorientational jumps amongst the eight corners of a cube (cubic tumbling) [30]:

$$\text{EISF} = \frac{1}{8} \left[1 + 3j_0\left(\frac{2}{\sqrt{3}}Qd_{\text{B-H}}\right) + 3j_0(Qd_{\text{H-H}}) + j_0(2Qd_{\text{B-H}}) \right]. \quad (3)$$

Finally, for isotropic rotational diffusion on the surface of a sphere with radius $d_{\text{B-H}}$ [28]:

$$\text{EISF} = j_0^2(Qd_{\text{B-H}}). \quad (4)$$

References

- [1] V. Stavila, L. Klebanoff, J. Vajo, P. Chen, Development of on-board reversible complex metal hydrides for hydrogen storage, in: L. Klebanoff (Ed.), *Hydrogen Storage Technology: Materials and Applications*, CRC Press, Boca Raton, 2013, pp. 133–211.
- [2] A. Unemoto, M. Matsuo, S. Orimo, *Adv. Funct. Mater.* 24 (2014) 2267–2279.
- [3] A. Remhof, Z. Łodziana, P. Martelli, O. Friedrichs, A. Züttel, A.V. Skripov, J.P. Embs, T. Strässle, *Phys. Rev. B* 81 (2010) 214304.
- [4] D. Blanchard, J.B. Maronsson, M.D. Riktor, J. Kheres, D. Sveinbjörnsson, E. Gil Bardají, A. Léon, F. Juranyi, J. Wuttke, K. Lefmann, B.C. Hauback, M. Fichtner, T. Vegge, *J. Phys. Chem. C* 116 (2012) 2013–2023.
- [5] N. Verdal, T.J. Udovic, J.J. Rush, X. Liu, E.H. Majzoub, J.J. Vajo, A.F. Gross, *J. Phys. Chem. C* 117 (2013) 17983–17995.
- [6] X. Liu, E.H. Majzoub, V. Stavila, R.K. Bhakta, M.D. Allendorf, D.T. Shane, M.S. Conradi, N. Verdal, T.J. Udovic, S.-J. Hwang, *J. Mater. Chem. A* 1 (2013) 9935–9941.
- [7] N. Verdal, T.J. Udovic, J.J. Rush, *J. Phys. Chem. C* 116 (2012) 1614–1618 (ibid. 5275–5275).
- [8] N. Verdal, T.J. Udovic, J.J. Rush, H. Wu, A.V. Skripov, *J. Phys. Chem. C* 117 (2013) 12010–12018.
- [9] W.H. Stockmayer, C.C. Stephenson, *J. Chem. Phys.* 21 (1953) 1311–1312.
- [10] P. Fisher, A. Züttel, *Mater. Sci. Forum* 443–444 (2004) 287–290.
- [11] G. Renaudin, S. Gomes, H. Hagemann, L. Keller, K. Yvon, *J. Alloys Comp.* 375 (2004) 98–106.
- [12] D.B. Ravnsbæk, L.H. Rude, T.R. Jensen, *J. Solid State Chem.* 184 (2011) 1858–1866.
- [13] J.E. Olsen, M.H. Sørby, B.C. Hauback, *J. Alloys Comp.* 509 (2011) L228–L231.
- [14] M. Matsuo, S. Kuromoto, T. Sato, H. Oguchi, H. Takamura, S. Orimo, *Appl. Phys. Lett.* 100 (2012) 203904.
- [15] R.D. Shannon, *Acta Cryst. A* 32 (1976) 751–767.
- [16] N.B., the corresponding Shannon crystal radius of the BH_4^- anion was calculated from the NaBH_4 lattice constant using the VI-coordinate Shannon crystal radius of the Na^+ cation.
- [17] All commercial suppliers in this paper are mentioned for clarity. This does not imply recommendation or endorsement by NIST.
- [18] A. Meyer, R.M. Dimeo, P.M. Gehring, D.A. Neumann, *Rev. Sci. Instrum.* 74 (2003) 2759–2777.
- [19] J.R.D. Copley, J.C. Cook, *Chem. Phys.* 292 (2003) 477–485.
- [20] T.J. Udovic, C.M. Brown, J.B. Leão, P.C. Brand, R.D. Jiggetts, R. Zeitoun, T.A. Pierce, I. Peral, J.R.D. Copley, Q. Huang, D.A. Neumann, R.J. Fields, *Nucl. Instrum. Meth. A* 588 (2008) 406–413.
- [21] R.T. Azuah, L.R. Kneller, Y. Qiu, P.L.W. Tregenna-Piggott, C.M. Brown, J.R.D. Copley, R.M. Dimeo, *J. Res. Natl. Inst. Stan.* 114 (2009) 341–358.
- [22] K. Momma, F. Izumi, *J. Appl. Crystallogr.* 44 (2011) 1272–1276.
- [23] T.J. Udovic, N. Verdal, J.J. Rush, D.J. De Vries, M.R. Hartman, J.J. Vajo, A.F. Gross, A.V. Skripov, *J. Alloys Comp.* 580 (2013) S47–S50.
- [24] P. Martelli, A. Remhof, A. Borgschulte, R. Ackermann, T. Strässle, J.P. Embs, M. Ernst, M. Matsuo, S. Orimo, Andreas Züttel, *J. Phys. Chem. A* 115 (2011) 5329–5334.
- [25] A.V. Skripov, A.V. Solonin, L.H. Rude, T.R. Jensen, Y. Filinchuk, *J. Phys. Chem. C* 116 (2012) 26177–26184.
- [26] A. Remhof, Z. Łodziana, F. Buchter, P. Martelli, F. Pendolino, O. Friedrichs, A. Züttel, J.P. Embs, *J. Phys. Chem. C* 113 (2009) 16834–16837.
- [27] N. Verdal, M.R. Hartman, T. Jenkins, D.J. DeVries, J.J. Rush, T.J. Udovic, *J. Phys. Chem. C* 114 (2010) 10027–10033.
- [28] M. Bée, *Quasielastic Neutron Scattering, Principles and Applications in Solid State Chemistry, Biology and Materials Science*, Adam Hilger, Bristol, 1988.
- [29] K. Sköld, *J. Chem. Phys.* 49 (1968) 2443–2445.
- [30] J.J. Rush, L.A.D. Graaf, R.C. Livingston, *J. Chem. Phys.* 58 (1973) 3439–3447.